PERGAMON

International Journal of Solids and Structures 36 (1999) 4543–4562

INTERNATIONAL JOURNAL OF SOLIDS and STRUCTURES

Development of a multiaxial fatigue theory by considering constraint effects on small mixed-mode cracks

Y. Wang[1], J. Pan*

Department of Mechanical Engineering and Applied Mechanics, The University of Michigan, Ann Arbor, MI 48109, U.S.A.

Received 18 January 1998; in revised form 9 July 1998

Abstract

The effects of the transverse strain (the normal strain in the crack-line direction) on the near-tip fields of small shallow surface cracks (Case A cracks) in power-law hardening materials are investigated by finite element analyses. The small Case A cracks are under plane stress, general yielding, and mixed mode I and II conditions. Constant effective stress contours representing the intense straining zones near the tip, deformed crack-tip profiles and near-tip mode mixity factors are presented for different transverse strains in the crack-line direction. Based on the concept of characterization of fatigue crack growth by the cyclic J-integral, the effects of the transverse strain on J are investigated. The results suggest that the fatigue life prediction based on multiaxial fatigue theories and the critical plane approach should include the constraint effects due to the transverse strain. Consequently, the concept of constant fatigue life contour on the Γ-plane in multiaxial fatigue theories is generalized to the constant fatigue life surface in the Γ-space where the shear strain and the two normal strains are the three axes. Finally, a damage parameter as a function of the shear strain and the two normal strains is proposed for evaluation of fatigue damage under multiaxial loading conditions.

1. Introduction

The strain-based low-cycle fatigue theories were initially developed in the late 1950s and early 1960s in response to the need to predict fatigue life where local plastic deformation occurs. Several strain-based multiaxial fatigue theories were proposed in the past, for example, see Garud (1981) and Brown and Miller (1982). Early works on fatigue theories involved correlations of fatigue life to the maximum principal strain range, the maximum shear strain range, and the maximum octahedral shear strain range. More recent approaches are based on the concept of the critical plane for crack initiation and growth (Fatemi and Socie, 1988; Socie, 1993).

* Corresponding author. Tel.: 001 734 764 9404; fax: 001 734 647 3170; e-mail: jwo@engin.umich.edu

[1] Present address: Meritor Automotive, Inc., 2135 West Maple Road, Troy, MI 48084, U.S.A.

0020-7683/99/$ - see front matter
PII: S0020-7683(98)00229-7

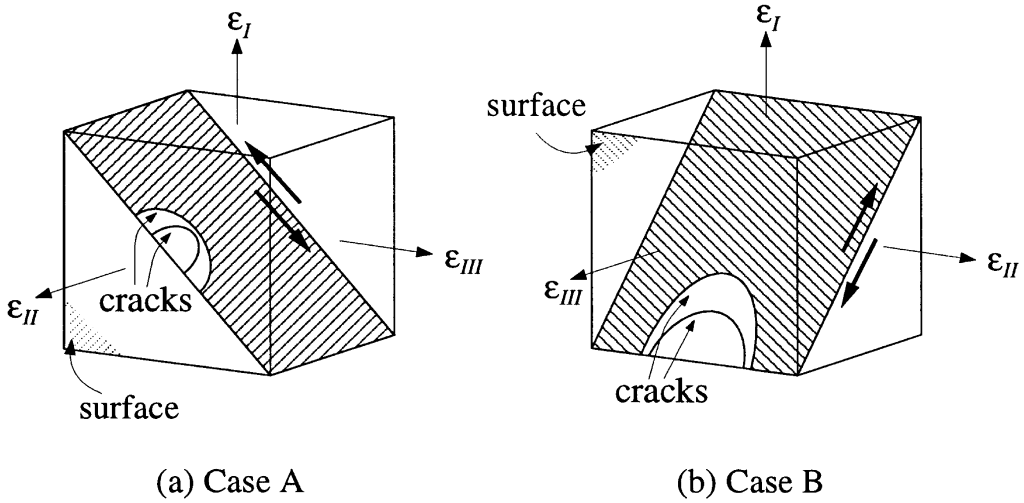

Fig. 1. Stage I crack growth direction for (a) Case A cracks, (b) Case B cracks.

Brown and Miller (1973) proposed a multiaxial fatigue theory based on the physical interpretation of the mechanisms of fatigue crack growth. Their theory can be represented graphically by contours of constant fatigue life on the Γ-plane. For a given life, the contour can be expressed mathematically by

$$\tfrac{1}{2}\gamma^* = f(\varepsilon_n^*) \tag{1}$$

where $\frac{1}{2}\gamma^*$ is the maximum shear strain and ε_n^* is the normal strain on the maximum shear strain plane. This equation underlines the strain parameters for correlating fatigue data, and indicates the importance of both the maximum shear strain and the tensile strain normal to the maximum shear strain plane. Two types of stage I fatigue cracks (Forsyth, 1961) are proposed: Case A for cracks propagating along the surface and Case B for cracks propagating away from the surface, as schematically shown in Fig. 1. In this fatigue, ε_I represents the maximum principal strain, ε_{II} is the second largest principal strain, and ε_{III} is the minimum principal strain. A specific form for eqn (1) was suggested for Case A cracks by Brown and Miller (1979) as

$$\left(\frac{\frac{1}{2}\gamma^*}{A}\right)^j + \left(\frac{\varepsilon_n^*}{B}\right)^j = 1 \tag{2}$$

where A, B and j are the empirical life-dependent functions. They suggested that $j = 2$ for ductile materials and 1 for brittle materials.

Lohr and Ellison (1980) proposed two modified fatigue parameters $\hat{\gamma}$ and $\hat{\varepsilon}_n$ where $\hat{\gamma}$ is the shear strain driving cracks through the thickness and $\hat{\varepsilon}_n$ is the normal strain on the $\hat{\gamma}$-plane. Therefore, for Case A cracks, $\frac{1}{2}\hat{\gamma} = \frac{1}{2}(\varepsilon_I - \varepsilon_{II})$ and $\hat{\varepsilon}_n = \frac{1}{2}(\varepsilon_I + \varepsilon_{II})$, where ε_{II} is used instead of ε_{III} in Brown and Miller's theory for Case A cracks. They also proposed a linear relationship

$$\hat{\gamma}+\kappa\hat{\varepsilon}_{\mathrm{n}}=\text{constant} \tag{3}$$

and suggested a value of 0.4 for κ.

Socie et al. (1985) investigated the effects of mean stress on fatigue crack growth since the tensile mean stresses normal to the crack surface should open the crack and assist the crack growth. Socie et al. (1985) proposed a modification of Lohr and Ellison's theory as

$$\hat{\gamma}+\kappa\hat{\varepsilon}_{\mathrm{n}}+\frac{\hat{\sigma}_{\mathrm{n}}}{E}=\text{constant} \tag{4}$$

and a modification of Kandil, Brown and Miller's (1982) theory as

$$\gamma^{*}+\mathscr{S}\varepsilon_{\mathrm{n}}^{*}+\frac{\sigma_{\mathrm{n}}^{*}}{E}=\text{constant} \tag{5}$$

Here, $\mathscr{S}$ is equal to 1.0, and $\hat{\sigma}_{\mathrm{n}}$ and σ_{n}^{*} represent the mean stress normal to $\hat{\gamma}$-plane and γ^{*}-plane, respectively.

Many research works on the effects of the shear strain, the normal strain and the mean stress on the shear plane have been carried out. However, the effects of the transverse strain (the normal strain in the crack-line direction) have not been accounted for damage accumulation, for example, in the formulation of multiaxial fatigue theory in conjunction with the critical plane approach in Chu et al. (1993) and Chu (1995), and in the fatigue life prediction of an automotive structural component based on the critical plane approach in Hou et al. (1998). In Wang and Pan (1996a), a small crack model with consideration of the transverse strain was presented. Their results showed a second concentration of plastic shearing directly below the crack tip and a larger crack opening displacement due to the tensile transverse strain. Therefore, in this paper, we examine the effects of the transverse strain on the near-tip fields of small Case A cracks in power-law strain hardening materials. Based on the concept of characterization of fatigue crack growth by the cyclic J-integral (Dowling and Begley, 1976; Dowling, 1977), we also investigate the effects of the transverse strain on J under plane stress, general yielding, and mixed mode I and II conditions.

2. Governing equation

To examine the implications of the mixed-mode crack-tip fields under monotonically increasing loading conditions to multiaxial fatigue theories, we here present an analysis based on a simple nonlinear material model. We consider a power-law strain hardening material with a uniaxial tensile stress–strain relation as

$$\frac{\varepsilon}{\varepsilon_0}=\alpha\left(\frac{\sigma}{\sigma_0}\right)^{n} \tag{6}$$

where ε is the tensile strain, σ is the tensile stress, ε_0 and σ_0 are the reference strain and stress (usually we take $\varepsilon_0=\sigma_0/E$ where E is Young's modulus), α is a material constant, and n is the strain hardening exponent. When n is equal to one, eqn (6) represents a linear elastic material. When n approaches infinity, eqn (6) gives a rigid-perfectly plastic behavior. However, the Ramberg–

Osgood law is usually used to describe the elastic–plastic behavior of materials under uniaxial tension:

$$\frac{\varepsilon}{\varepsilon_0} = \frac{\sigma}{\sigma_0} + \alpha \left(\frac{\sigma}{\sigma_0}\right)^n \tag{7}$$

The Ramberg–Osgood law can be generalized to multiaxial states. Here, the strain ε_{ij} can be written as the sum of an elastic part ε_{ij}^{e} and a plastic part ε_{ij}^{p}:

$$\varepsilon_{ij} = \varepsilon_{ij}^{e} + \varepsilon_{ij}^{p} \tag{8}$$

with

$$\varepsilon_{ij}^{e} = \frac{1+v}{E} s_{ij} + \frac{1-2v}{3E} \sigma_{kk} \delta_{ij} \tag{9}$$

$$\varepsilon_{ij}^{rp} = \frac{3}{2} \alpha \left(\frac{\sigma_e}{\sigma_0}\right)^{n-1} \frac{s_{ij}}{\sigma_0} \tag{10}$$

where v is Poisson's ratio, s_{ij} are the deviatoric stresses, which are defined as $s_{ij} = \sigma_{ij} - \frac{1}{3}\sigma_{kk}\delta_{ij}$, and $\sigma_e (= (\frac{3}{2} s_{ij} s_{ij})^{1/2})$ is the effective stress. Here, i and j have a range of 1 to 3 and the summation convention is adopted for repeated indices. Also, the effective plastic strain ε_e is defined here as $\varepsilon_e = (\frac{2}{3} \varepsilon_{ij}^{p} \varepsilon_{ij}^{p})^{1/2}$.

Consider a cracked body where the elastic strain components are negligible compared to their plastic counterparts. Therefore, eqn (10) can be adequately used to describe the stress–strain behavior with assumption of deformation plasticity theory with power-law hardening. Now we consider that the cracked body is subjected to tractions along the boundary. The tractions are scaled by a loading parameter P. Then Il'yushin's theory (Il'yushin, 1946) gives

$$\sigma_{ij} = P \sigma'_{ij}(x_i, n) \tag{11}$$

$$\varepsilon_{ij} = \alpha \left(\frac{P}{\sigma_0}\right)^n \varepsilon'_{ij}(x_i, n) \tag{12}$$

where x_i is the coordinate of the material element. The quantities σ'_{ij} and ε'_{ij} are functions of x_i and n, and are independent of P. This result follows from the homogeneous nature of the equations of equilibrium, compatibility and the constitutive relation. Since the stress and strain fields increase proportionally at every point, the fully plastic solution based upon deformation plasticity theory coincides with the solution for the corresponding incremental or flow theory.

The path-independent J-integral was introduced by Rice (1968). Since the integrand of the J-integral involves the products of stresses and displacement gradients, based on eqn (11) and (12), the fully plastic J will be proportional to P^{n+1}. Then the J-integral for power-law hardening materials can be expressed as

$$J_p = \alpha \varepsilon_0 \sigma_0 a h \left(\frac{a}{w}, n\right) \left(\frac{P}{P_0}\right)^{n+1} \tag{13}$$

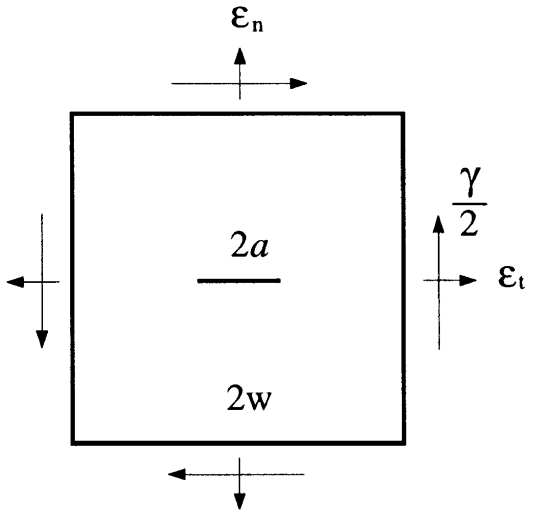

Fig. 2. A center cracked panel subjected to biaxial normal and shear strains.

where P_0 is a reference load in terms of σ_0, a is the crack length, and w is the other significant length parameter. Here the subscript p is used to designate power-law material behavior. The dimensionless function h depends on a/w, n, and possible other normalized geometric parameters, but is independent of P. This equation will be used later to derive the relationship between J and the boundary loading conditions in our finite element analysis.

3. Finite element model

We consider a center cracked panel under plane stress, multiaxial loading conditions, as shown in Fig. 2. A coordinate system is selected such that the x-axis is in the crack-line direction. The center cracked panel is subject to combined biaxial normal and shear strains with respect to the x–y coordinate system. In the figure, $2a$ represents the crack length, $2w$ represents the width of the panel, γ represents the engineering shear strain, ε_n represents the normal strain perpendicular to the crack, and ε_t represents the transverse strain which is the normal strain in the crack-line direction. The crack is subjected to both the opening and shear modes, and therefore is under mixed-mode (I and II) loading conditions.

The entire domain shown in Fig. 2 is discretized into eight-node quadrilateral elements for our finite element model due to the crack geometry and the loading conditions. Figure 3(a) shows only a quarter of the finite element model. The near-tip region is shown in Fig. 3(b). In the immediate crack-tip region, we have a ring of 32 wedge-shaped elements. Collapsed nodes resulting in the $1/r$ singularity are used for these wedge-shaped elements. The entire finite element model consists of 1488 elements and 4620 nodes. In this study, we are interested in the near-tip fields of small cracks under general yielding conditions. Therefore, the ratio of a/w is taken as 0.02 to ensure that the effect of the plastic flow near the crack tip of the remote boundary is minimum.

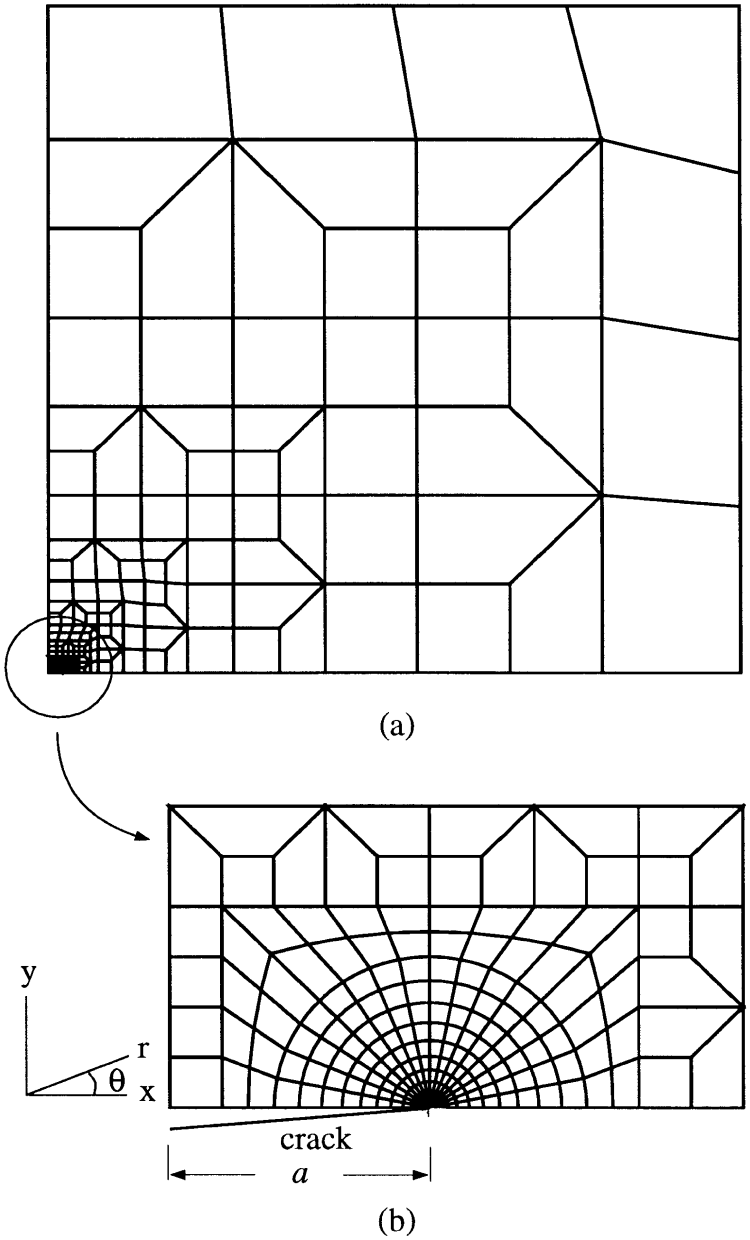

Fig. 3. (a) A finite element model for a quarter of a center cracked plate, (b) the near-tip region.

Along the remote boundary, the displacements are prescribed according to the applied strain fields. Based on the small-strain theory, the strains are related to the displacements as

$$\varepsilon_{ij} = \frac{1}{2}\left(\frac{\partial u_i}{\partial x_j} + \frac{\partial u_j}{\partial x_i}\right) \tag{14}$$

Here, u_i are the displacements in the x_i-directions. This equation is used to translate the applied strains into the displacements along the boundary.

All our computations are performed using the finite element code ABAQUS (Version 5.5). We choose the Ramberg–Osgood material behavior to describe the material deformation plasticity behavior. We select $n = 3$ to represent high-hardening materials, $n = 10$ to represent low-hardening materials, and $n = 20$ to approximate perfectly-plastic materials. Also we select the material constants such that the elastic strains are small and negligible compared with the plastic strains when the stresses are large. Therefore, our solutions can be used to approximate those for pure power-law strain hardening materials.

4. Mixed-mode crack-tip fields

For various combinations of the applied strains along the boundary, the near-tip stress and strain fields are investigated. To understand the effects due to the boundary strains on the crack-tip fields, we here define two strain parameters. The first parameters is the applied strain ratio ϕ which is the ratio of the normal strain ε_n to the shear strain $\frac{1}{2}\gamma$ as shown in Fig. 2, is consistent with the multiaxial fatigue theories (Wang and Pan, 1996a), as

$$\phi = \frac{\varepsilon_n}{\frac{1}{2}\gamma} \tag{15}$$

The second parameter is the constraint ratio ζ which is the ratio of the transverse strain ε_t to the shear strain $\frac{1}{2}\gamma$ as

$$\zeta = \frac{\varepsilon_t}{\frac{1}{2}\gamma} \tag{16}$$

Note that the two strain parameters are normalized by the shear strain due to the fact that the shear strain is considered as the primary driving force for fatigue crack growth in multiaxial fatigue theories (for example, see Chu et al., 1993; Chu 1995).

On the other hand, in nonlinear fracture mechanics, the constraint effect is expressed in terms of the transverse stress, for example, see O'Dowd and Shih (1991; 1992). For the center cracked panel subject to mixed mode I and II loading conditions without the transverse stress, the material incompressibility gives $\zeta = -\frac{1}{2}\phi$. For the panel subject to pure model II loading conditions, $\zeta = 0$ and $\phi = 0$. For the panel subject to combined equal biaxial normal and shear strains (Wang and Pan, 1996a), $\zeta = \phi$. This is the case that the crack growth is in the maximum shear strain direction as discussed in Brown and Miller (1973). With consideration of different combinations of ϕ and ζ, the constraint effects due to the transverse strain can be explored systematically.

In our finite element computations, we set $\nu = 0.4999$, $\alpha = 1$, and $E/\sigma_0 = 1.0 \times 10^4$ for the Ramberg–Osgood stress–strain law to approximate the behavior of pure power-law strain hardening materials. We consider the materials with the hardening exponent n equal to 3, 10 and 20. We show the results of three applied strain ratios $\phi = 1/3$, $1/6$, and 0 under various constraint ratio ζ from $-1/2$ to $1/2$. Here, we only show the computational results of $n = 3$ and $n = 10$.

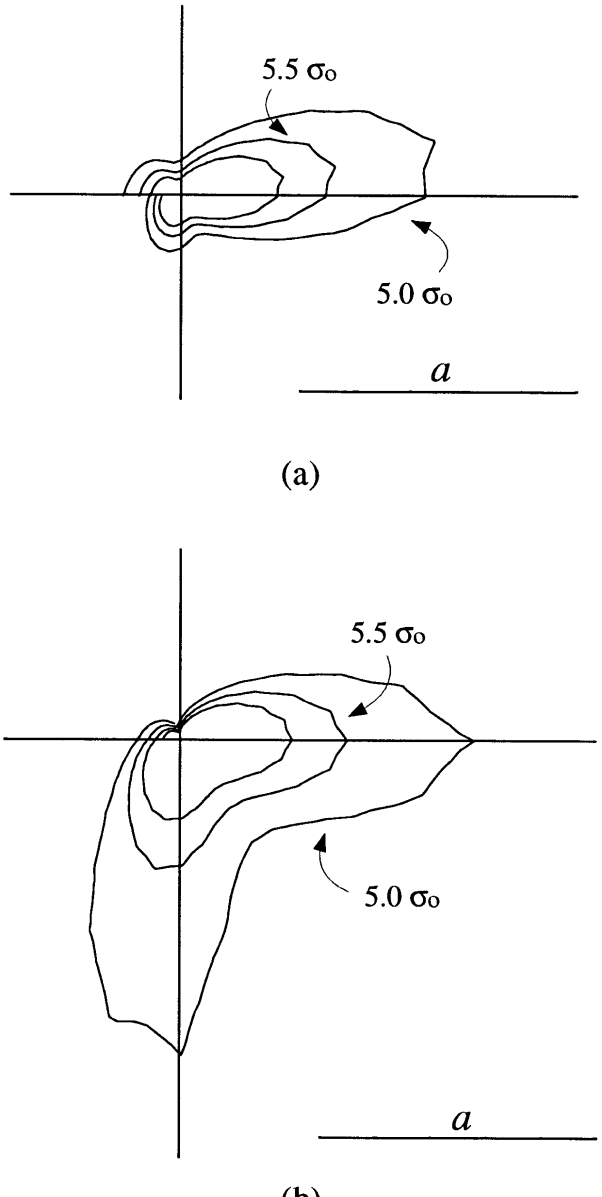

Fig. 4. Effective stress contours for $n = 3$ and $\phi = 1/3$ at $\varepsilon_n = 0.002$. (a) Uniaxial tension and shear ($\zeta = -1/6$), (b) equal biaxial tension and shear ($\zeta = 1/3$).

Figure 4 shows the effective stress contours representing the intense straining zones near the crack tip for $n = 3$ and $\phi = 1/3$. Figure 4(a) shows the effective stress contours under uniaxial tensile and shear strain at $\varepsilon_n = 0.002$, $\varepsilon_t = -0.001$ and $\gamma/2 = 0.006$. Note that when the center cracked panel is subject to $\varepsilon_n = 0.002$ and $\gamma/2 = 0.006$, this combination of strains corresponds to

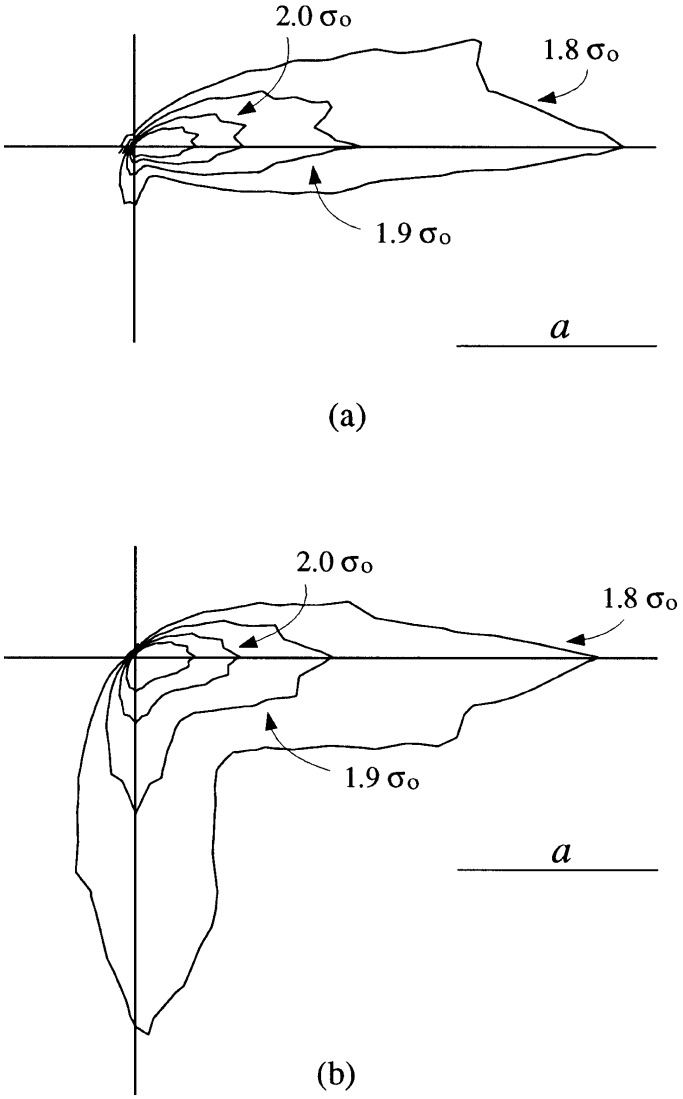

Fig. 5. Effective stress contours for $n = 10$ and $\phi = 1/3$ at $\varepsilon_n = 0.004$. (a) Uniaxial tension and shear ($\zeta = -1/6$), (b) equal biaxial tension and shear ($\zeta = 1/3$).

$\phi = 1/3$. When the transverse stress σ_t is equal to 0, the panel without the small crack should have $\varepsilon_t = -0.001$ according to the material incompressibility. This gives $\zeta = -1/6$. Figure 4(a) indicates that the plastic shearing is mostly concentrated directly ahead of the tip even under mixed-mode loading conditions. Figure 4(b) shows the effective stress contours for $\varepsilon_n = 0.002$, $\varepsilon_t = 0.002$ and $\gamma/2 = 0.006$. This is the case of equal biaxial tensile and shear loading conditions corresponding to $\phi = \zeta = 1/3$. For this case, the transverse stress σ_t is equal to the normal stress σ_n. This figure indicates that plastic shearing appears not only directly ahead of the tip but also directly below the tip. Figure 5 shows the corresponding cases for $n = 10$ at $\varepsilon_n = 0.004$. As shown in this figure,

the effective stress contours for these combinations of ϕ and ζ under mixed-mode loading conditions are quite similar to those shown in Fig. 4. However, the intensity of the second concentration of plastic shearing depends upon n and ζ, as indicated by our computational results. As the transverse strain becomes negative, the second concentration of plastic shearing becomes smaller as shown in these figures. It should be noted that for a given combination of n, ϕ and ζ, these effective stress contours are not exactly self-similar as they should be for pure power-law strain hardening materials because the small elastic contribution in the Ramberg–Osgood stress–strain relation that we used in ABAQUS.

Figure 6 shows the deformed shapes of the crack-tip profiles for $n = 3$ and $\phi = 1/3$. Figure 6(a) shows the deformed shape under uniaxial tensile and shear loads at $\varepsilon_n = 0.008$, $\varepsilon_t = -0.004$ and $\gamma/2 = 0.024$ ($\zeta = -1/6$). Figure 6(b) shows the deformed shape under equal biaxial tensile and shear loads at $\varepsilon_n = 0.008$, $\varepsilon_t = 0.008$ and $\gamma/2 = 0.024$ ($\zeta = 1/3$). As shown in the figure, the case with the tensile transverse stress (Fig. 6(b)) apparently has more crack opening displacement than that without the tensile transverse stress (Fig. 6(a)). Figure 7 shows the corresponding results for $n = 10$ at $\varepsilon_n = 0.008$. As shown in Fig. 7, the deformed shapes of the crack-tip profiles for these combinations of ϕ and ζ have the similar trends as those shown in Fig. 6.

The radial and angular dependence of the crack-tip fields for the center cracked panel under mixed-mode loading conditions has been studied thoroughly in Wang and Pan (1998b). In this paper, we choose not to present the detailed angular variation of the crack-tip fields for different ratios of ζ for consideration of the length of the paper. Instead, we examine the near-tip mode mixity factor M^p (Shih, 1973) under different constraint ratios of understand the effects of the transverse strain on the opening stress and shear stress directly ahead of the crack tip. The near-tip mixity factor M^p (Shih, 1973) is defined as

$$M^p = \frac{2}{\pi}\tan^{-1}\left[\lim_{r\to 0}\frac{\sigma_{\theta\theta}(r,\theta=0)}{\sigma_{r\theta}(r,\theta=0)}\right] \tag{17}$$

Here, $\theta = 0$ represents the direction directly ahead of the tip. Under pure mode I condition, $M^p = 1$. Under pure mode II condition, $M^p = 0$. M^p has a value between 0 and 1 under mixed mode I and II conditions.

Figure 8 shows M^p as a function of $(2/\pi)\tan^{-1}\phi$ for $n = 3$. The values of M^p are sampled at the radial distance about $2J/\sigma_0$ of the crack tip (O'Dowd and Shih, 1991, 1992). Note that the small-strain finite element results in general are not valid at radial distances smaller than $2J/\sigma_0$ due to large deformation near crack tips. Therefore, the stresses at this radial distance $2J/\sigma_0$ are usually used to investigate the constraint effects (O'Dowd and Shih, 1991, 1992). Two different constraint cases are considered. One is under equal biaxial normal and shear strain ($\zeta = \phi$) and the other one is without any transverse stress such that $\zeta = -\frac{1}{2}\phi$. As shown in Fig. 8, M^p for $\zeta = \phi$ is substantially larger than that for $\zeta = -\frac{1}{2}\phi$ under mixed-mode loading conditions. This indicates that the presence of a tensile transverse strain results in more opening stress ahead of the tip. This is consistent with the results shown in Figs. 6 and 7 where the cases with the tensile transverse stress have more opening displacement than the cases without the transverse stress. Figure 9 shows the corresponding results for $n = 10$. This figure shows the same trends as those in Fig. 8. As shown in both figures, the strain hardening exponent n does have some effects on the trend. Also, it is clear from Figs. 8 and 9 that the near-tip fields for Case A cracks are dominated by shear ahead of the tip since the values of M^p are less than 0.6 for the cases with and without constraints.

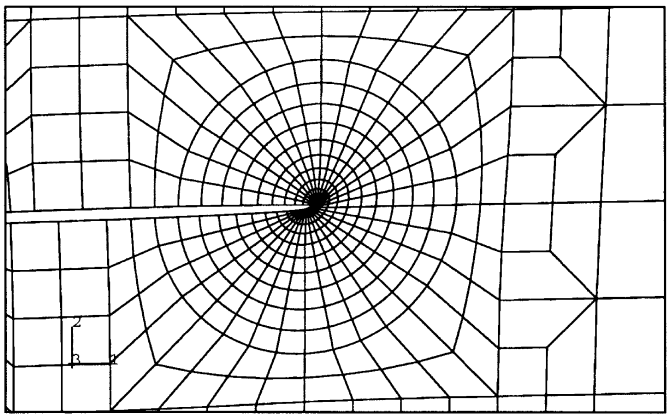

(a)

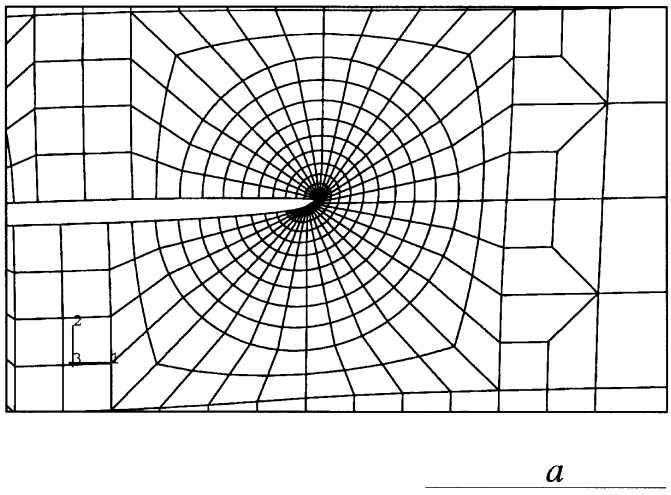

(b)

Fig. 6. Deformed crack-tip profiles for $n = 3$ and $\phi = 1/3$ at $\varepsilon_n = 0.008$. (a) Uniaxial tension and shear ($\zeta = -1/6$), (b) equal biaxial tension and shear ($\zeta = 1/3$).

As indicated in Dowling (1977) and Dowling and Begley (1976) for mode I fatigue cracks and as shown in Wang and Pan (1996a, 1996b, 1998a, 1998b) for mixed-mode fatigue cracks, the cyclic J-integral can be used to characterize fatigue growth data and fatigue life data. Therefore we examine the values of J under different transverse strains to understand the implications of the transverse strain on the fatigue crack growth propensity. Figure 10 shows the value of J as a function of the constraint ratio ζ for $n = 3$ and the applied strain ratio $\phi = 0$, 1/6 and 1/3. In the

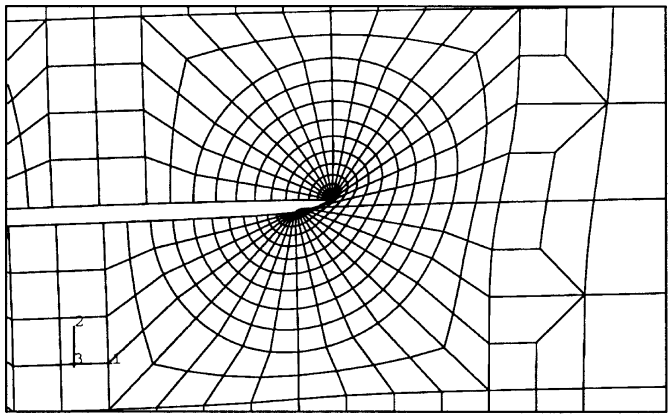

(a)

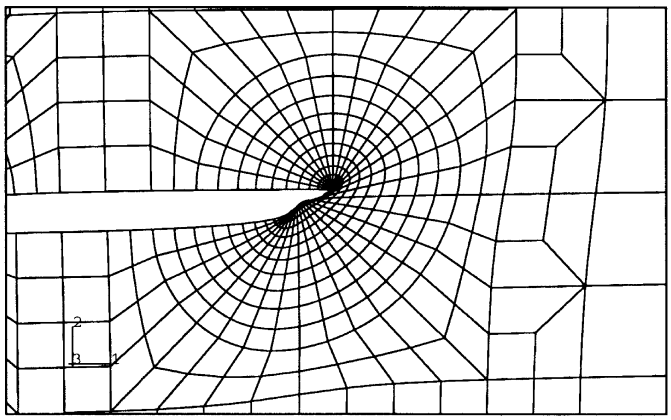

(b)

Fig. 7. Deformed crack-tip profiles for $n = 10$ and $\phi = 1/3$ at $\varepsilon_n = 0.008$. (a) Uniaxial tension and shear ($\zeta = -1/6$), (b) equal biaxial tension and shear ($\zeta = 1/3$).

figure, the values of J are normalized by J_0, which is defined as the value of J under pure shear load (pure mode II case). For the applied strain ratio $\phi = 0$, the results are not presented at ζ less than zero because the crack surfaces are in contact due to the applied compressive transverse strains from out finite element analysis. The contact phenomenon also exists for $\phi = 1/6$ at ζ less than about $-1/3$ and $\phi = 1/3$ at ζ less than about $-1/2$. In the figure, the symbol $\square$ represents the cases of the loading conditions without transverse stress ($\zeta = -\frac{1}{2}\phi$ from the material incompressibility). These cases are: $\phi = 0$ (pure mode II) and $\zeta = 0$; $\phi = 1/6$ and $\zeta = -1/12$; and $\phi = 1/3$

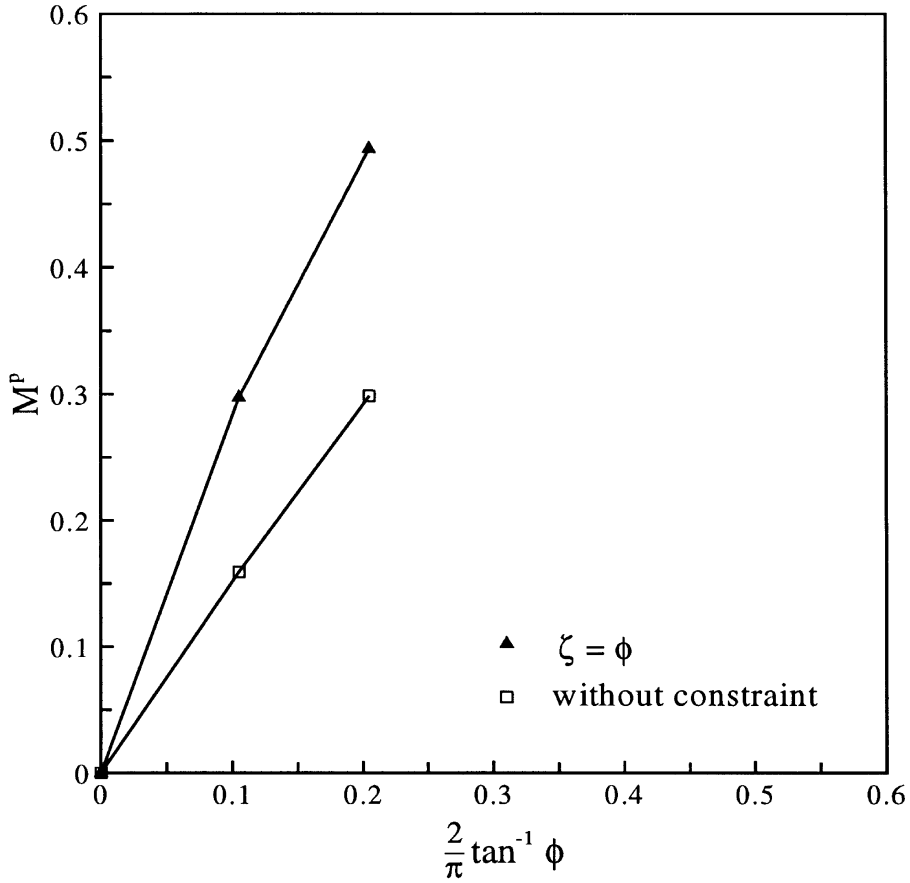

Fig. 8. Relationship between the near-tip mixity factor M^p and the strain ratio factor $(2/\pi)\tan^{-1}\phi$ at $n = 3$.

and $\zeta = -1/6$. The symbol ▲ represents the cases under equal biaxial tensile and shear loading conditions with $\phi = \zeta$. These are the cases where cracks grow in the direction of the maximum shear strain as discussed in Brown and Miller (1973). These cases are investigated by Wang and Pan (1996a) where the values of J are well correlated to the experimental fatigue lives for Case A cracks presented in Brown and Miller (1973). Figure 10 shows that the values of J increase as the constraint ratio ζ increases. As ϕ becomes as large as 1/3, J can change 100% as ζ varies. Figure 11 shows the corresponding results for $n = 10$. The results shown in this figures indicate the same trends as shown in Fig. 10 for $n = 3$.

5. Implications to multiaxial fatigue theories

Wang and Pan (1996a, 1996b, 1998a, 1998b) attempted to correlate the results of near-tip stress and strain fields of small cracks from the plastic fracture mechanics viewpoint to multiaxial low-cycle fatigue theories. They considered a small Case A crack model and assumed the fatigue crack

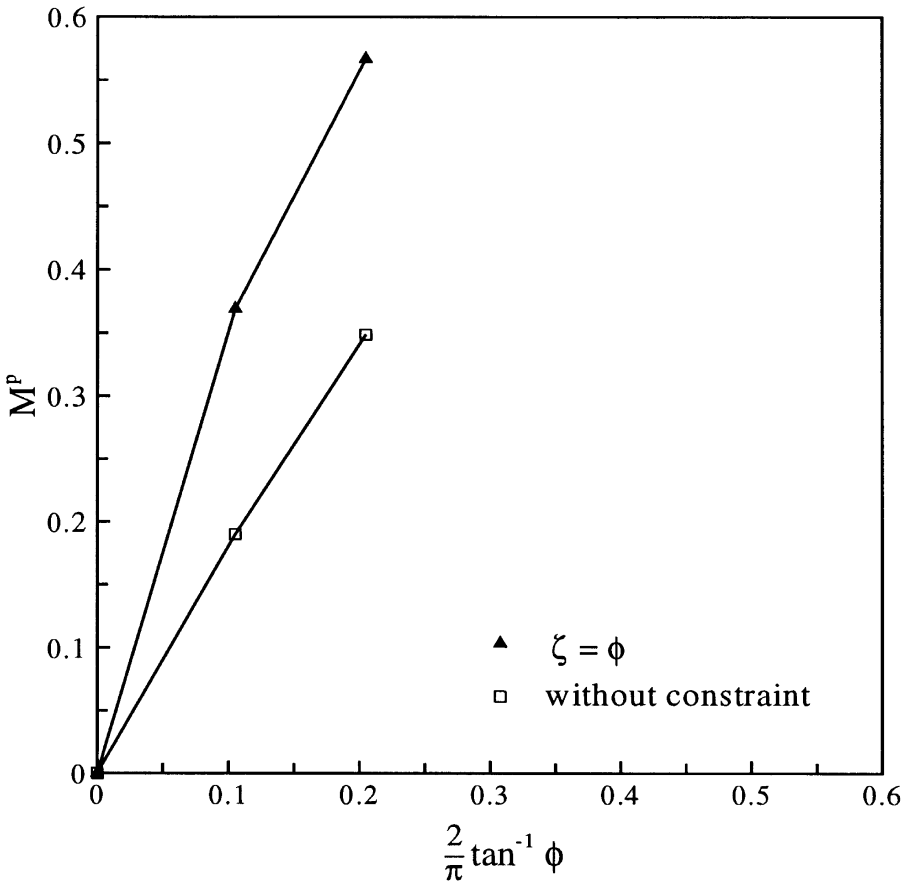

Fig. 9. Relationship between the near-tip mixity factor M^p and the strain ratio factor $(2/\pi)\tan^{-1}\phi$ at $n = 10$.

in the direction of the maximum shear strain (Wang and Pan, 1996a, 1998b). They presented the constant J-contours on the Γ-plane as shown in Fig. 12 for power-law strain hardening materials. They found that the general trends of the constant J-contours on the Γ-plane, instead of parameters as combinations of near-tip stresses and strains, agree well with those of the experimental constant fatigue lives on the Γ-plane as presented in Brown and Miller (1979) for 1%Cr–Mo–V steel. As clearly shown in Figs. 4 and 5, the intensity of the second concentration of plastic shearing directly below the crack tip becomes large when the tensile transverse stress is applied. This observation motivates us to investigate the effects of the transverse strain on the mixed-mode near-tip fields of small cracks. Based on the concept of characterization of fatigue crack growth by the cyclic J-integral, supported by the experimental results for mode I cracks by Dowling and Begley (1976) and Dowling (1977) and correlated by the computational results for mixed-mode cracks by Wang and Pan (1996a, 1998b) as shown in Fig. 12, we investigate the effects of the transverse strain on the values of J. As shown in Figs. 10 and 11, J increases as ζ increases. This trend is consistent under different combinations of ϕ and ζ. The strain hardening exponent n does have some effects on the general trend.

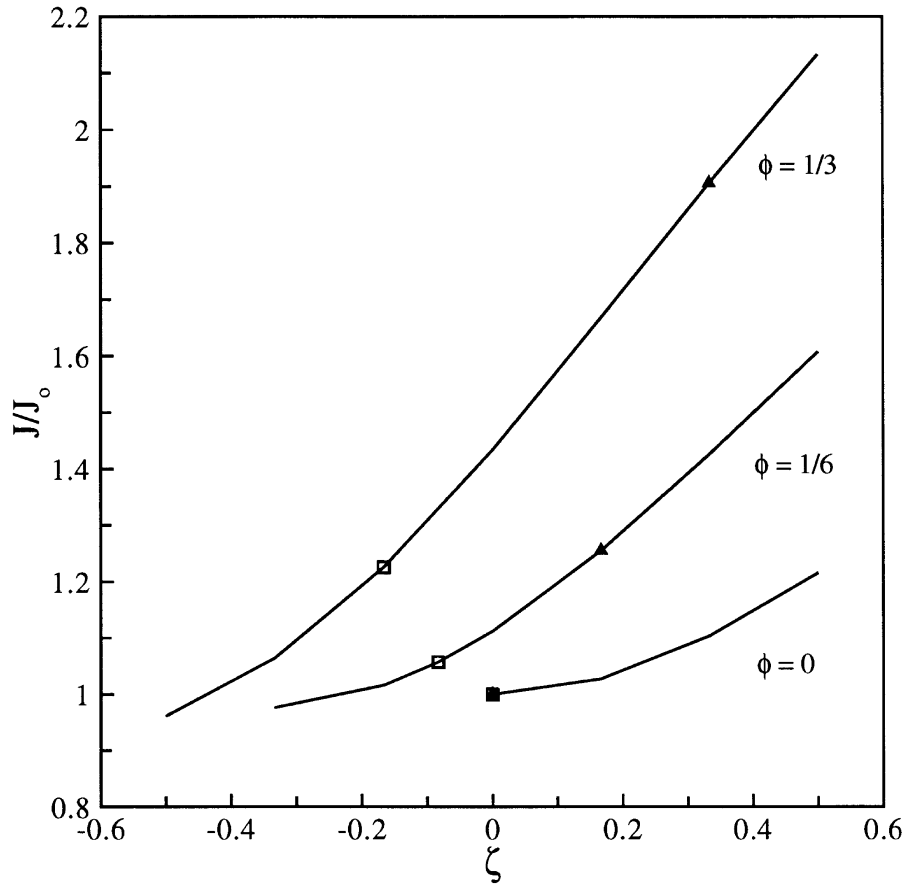

Fig. 10. J as a function of ζ for $n = 3$ and several values of ϕ.

Now we try to link the results of our small crack model to the prediction of damage accumulation based on multiaxial theories and the critical plane approach. The critical plane approach has been widely adopted to predict fatigue life under multiaxial loading conditions. The approach involves the assumption of many possible planes where the fatigue damage are evaluated. In contrast to most laboratory testing programs where fixed ratios of stresses or strains are applied under cyclic loading conditions, the critical material elements of structural components may be subject to truly multiaxial non-proportional cyclic loading conditions. When the critical plane approach is adopted, the damage parameter is assessed in consistent with those testing results under proportional cyclic loading conditions where small fatigue cracks appear in the maximum shear strain directions as in Socie et al. (1985) and Brown and Miller (1973). Correlations of experimental data suggest that using the shear strain and the normal strain on the maximum shear strain plane as the damage parameter seems to be reasonable and consistent. Many multiaxial fatigue theories have been proposed accordingly (Brown and Miller, 1979; Lohr and Ellison, 1980; Kandil et al., 1982, Socie et al., 1985). However, the effects of the transverse strain have not been considered for damage

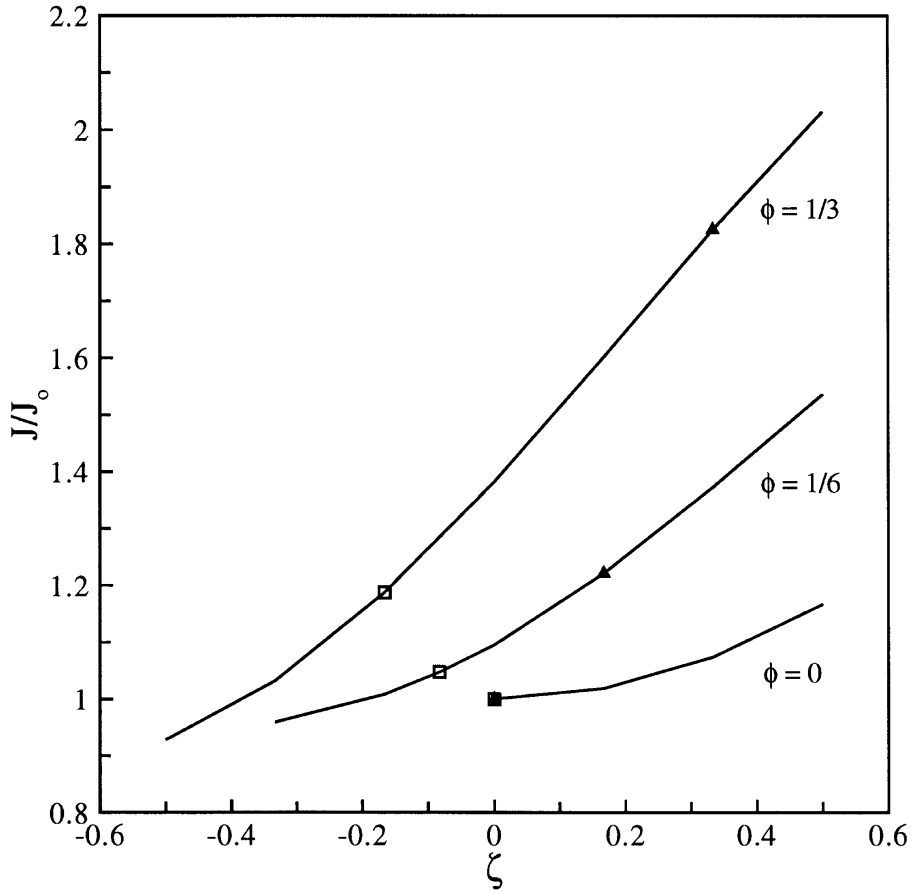

Fig. 11. J as a function of ζ for $n = 10$ and several values of ϕ.

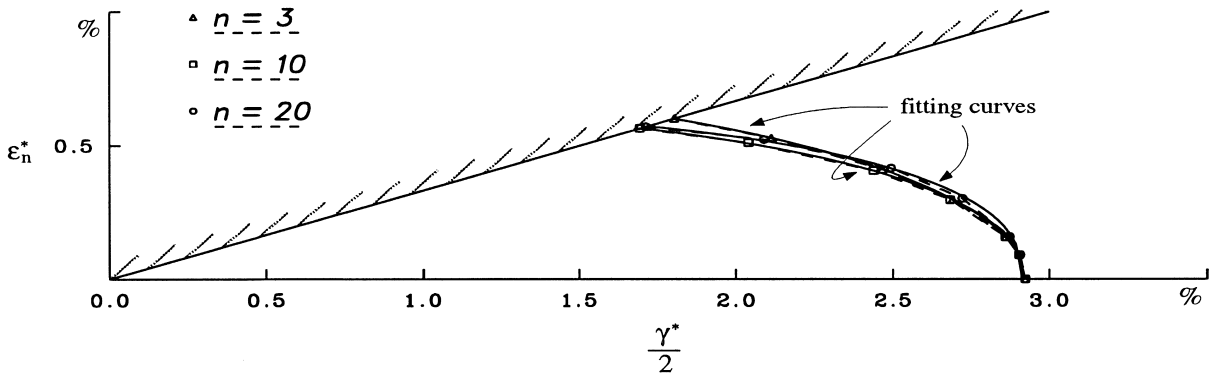

Fig. 12. The constant J contours on the Γ-plane. Here the solid lines are fitting curves.

accumulation based on the multiaxial fatigue theories in conjunction with the critical plane approach, see Chu et al. (1993) and Chu (1995). As shown in our present computational results, the transverse strain has significant effects on the crack-tip opening stress, opening displacement and the value of J. Therefore, the transverse strain should be considered in the multiaxial fatigue theories in conjunction with the critical plane approach.

We now examine the linear elastic case ($n = 1$) as detailed in the Appendix to understand the effects of the transverse strain on the value of J-integral. Equation (A6) in the Appendix is now presented here again:

$$\frac{J}{E\pi a} = \left(\frac{\gamma/2}{1+v}\right)^2 + \left(\frac{\varepsilon_n}{1-v^2} + \frac{v\varepsilon_t}{1-v^2}\right)^2 \tag{18}$$

As indicated in eqn (18), the transverse strain ε_t does have effect on the value of the J-integral. It should be noted that the contribution of the transverse strain on the value of J-integral is not as much as that of the normal strain ε_n because a factor of v is in front of ε_t as indicated in eqn (18). When $\varepsilon_n = \varepsilon_t$, this is the case where the crack is in the direction of the maximum shear strain. Denote the strains for this case by $\gamma^*/2$ and ε_n^*. Equation (18) then becomes

$$\frac{J}{E\pi a} = \left(\frac{\gamma^*/2}{1+v}\right)^2 + \left(\frac{\varepsilon_n^*}{1-v}\right)^2 \tag{19}$$

This equation has been derived in Wang and Pan (1998b).

Chu et al. (1993) presented a damage parameter D for the critical plane approach as

$$D = \gamma + \mathscr{S}\varepsilon_n \tag{20}$$

where $\mathscr{S}$ is a material constant, γ and ε_n represent the amplitudes of the shear strain and the normal strain, respectively. Note that D is expressed as a linear combination of γ and ε_n. However, as shown in Wang and Pan (1996a, 1998b), the constant J contours for power-law strain hardening materials on the Γ-plane are fitted well by a nonlinear power function of the maximum shear strain γ^* and the corresponding normal strain ε_n^* as

$$\left(\frac{\frac{1}{2}\gamma^*}{A}\right)^m + \left(\frac{\varepsilon_n^*}{B}\right)^m = 1 \tag{21}$$

where m varies from 2 to 2.53 for $n = 1$ to $n = 20$. The ratio A/B depends on n. The magnitudes of A and B depend on the values of γ^* and ε_n^*. The shapes of the constant J contours in general agree well with those of the nonlinear constant fatigue life curves on the Γ-plane presented in Brown and Miller (1973). The nonlinear constant fatigue life curves on the Γ-plane can be approximated by a nonlinear equation similar to eqn (21) as

$$\gamma^{*m} + \mathscr{T}\varepsilon_n^{*m} = \mathscr{V} \tag{22}$$

where $\mathscr{T}$ and $\mathscr{V}$ are the best-fit material constants for a given fatigue life. Along a constant fatigue life curve, the fatigue damage parameter D can be considered to be the same. Therefore, a natural selection of a damage parameter D, motivated by eqns (20) and (22), would be

$$D = (\gamma^{*m} + \mathscr{T}\varepsilon_n^{*m})^{1/m} \tag{23}$$

Equation (23) should reduce to eqn (20) when $m = 1$.

One possible way to include the effects of the transverse strain would be to add the transverse strain contribution into the expression of the damage parameter D. Based on eqn (23) for power-law hardening materials and eqn (18) for $n = 1$, a possible modification of D to include the constraint effect can be expressed as

$$D = (\gamma^m + (\mathscr{Q}\varepsilon_n + \mathscr{R}\varepsilon_t)^m)^{1/m} \tag{24}$$

where m, $\mathscr{Q}$ and $\mathscr{R}$ are material constants. For the linear elastic case ($n = 1$), m could be equal to two and $\mathscr{R}$ could be equal to $v\mathscr{Q}$ as suggested in eqn (18). When n is not equal to one, more computational or experimental results are needed to find an optimal set of m, $\mathscr{Q}$ and $\mathscr{R}$. The values of m can be close to those in Wang and Pan (1996a, 1998b) for cracks in the maximum shear strain direction where $\varepsilon_t = \varepsilon_n$. Since we propose the damage parameter D in terms of the three strains as in eqn (24), we essentially generalize the concept of constant fatigue life contour on the Γ-plane proposed by Brown and Miller (1973) to constant fatigue life surface in the Γ-space where $\gamma/2$, ε_n and ε_t are the three axes. Further experimental results and modeling effort should quantify the effects of the transverse strain on fatigue crack growth rate or fatigue damage assessment.

6. Conclusions

In this paper, a small crack model is proposed to examine the effects of the transverse strain (the normal strain in the crack-line direction) on the near-tip fields. We present the constant effective stress contours, the deformed crack-tip profiles and the mode mixity factors under different transverse strains. Based on the concept of characterization of fatigue crack growth by the cyclic J-integral, we also present the values of J under different transverse strains. The computational results show that J increases as the transverse strain increases and the strain hardening exponent n does have some effects on the trend. The results suggest that the fatigue life prediction based on multiaxial fatigue theories and the critical plane approach should include the effects of the transverse strains on fatigue crack growth propensity. Consequently, the concept of constant fatigue life contour on the Γ-plane in multiaxial fatigue theories is generalized to the constant fatigue life surface in the Γ-space where the shear strain and the two normal strains are the three axis. Finally, a damage parameter as a function of the shear strain and the two normal strains is proposed for evaluation of fatigue damage under multiaxial loading conditions.

Appendix

Consider a center cracked panel as shown in Fig. 2. Here we consider the case of $n = 1$. As the ratio a/w approaches to 0, the stress intensity factor K_I and K_{II} due to the remote normal stress σ_n and shear stress τ, which are perpendicular to and parallel to the crack, are

$$K_I = \sigma_n\sqrt{\pi a} \tag{A1}$$

$$K_{II} = \tau\sqrt{\pi a} \tag{A2}$$

The energy release rate J is related to K_I and K_{II} under plane stress conditions as

$$J = \frac{1}{E}(K_I^2 + K_{II}^2) \tag{A3}$$

For the case as shown in Fig. 2 under the normal stress σ_n and the shear stress τ, Hooke's law gives

$$\sigma_n = \frac{E}{1-v^2}\varepsilon_n + \frac{vE}{1-v^2}\varepsilon_t \tag{A4}$$

$$\tau = \frac{E}{1+v}\left(\frac{\gamma}{2}\right) \tag{A5}$$

Combining eqns (A1) to (A5) gives

$$\frac{J}{E\pi a} = \left(\frac{\gamma/2}{1+v}\right)^2 + \left(\frac{\varepsilon_n}{1-v^2} + \frac{v\varepsilon_t}{1-v^2}\right)^2 \tag{A6}$$

Equation (A6) clearly indicates that ε_t affects the value of J-integral. However, the effect of ε_t will not be as much as that of ε_n because there is a factor of v for the contribution of ε_t when compared to that of ε_n.

References

Brown, M.W., Miller, K.J. 1973. A theory for fatigue failure under multiaxial stress–strain conditions. Proceedings, Institution of Mechanical Engineers 187, 745–755.

Brown, M.W., Miller, K.J., 1979. High temperature low cycle biaxial fatigue of two steels. Fatigue of Engineering Materials and Structures 1, 217–229.

Brown, M.W., Miller, K.J. 1982. Two decades of progress in the assessment of multiaxial low-cycle fatigue life. Low-Cycle Fatigue and Life Prediction, ASTM STP 770. American Society of Testing and Materials, Philadelphia, pp. 482–499.

Chu, C.-C., 1995. Fatigue damage calculation using the critical plane approach. Journal of Engineering Materials and Technology 117, 41–49.

Chu, C.-C., Conle, F., Bonnen, J., 1993. Multiaxial stress–strain modeling and fatigue life prediction for sae axle shafts. Advances in Multiaxial Fatigue, ASTM STP 1191. American Society of Testing and Materials, Philadelphia, pp. 37–54.

Dowling, N.E., 1977. Crack growth during low-cycle fatigue of smooth axial specimens. Mechanics of Crack Growth, ASTM STP 637. American Society of Testing and Materials, Philadelphia, pp. 97–121.

Dowling, N.E., Begley, J.A., 1976. Fatigue crack growth during gross plasticity and the J-integral. Mechanics of Crack Growth, ASTM STP 590. American Society of Testing and Materials, Philadelphia, pp. 82–103.

Fatemi, A., Socie, D.F., 1988. A critical plane approach to multiaxial fatigue damage including out-of-phase loading. Fatigue and Fracture of Engineering Materials and Structures 11, 149–165.

Forsyth, P.J.E., 1961. A two-stage process of fatigue crack growth. Proceedings, Crack Propagation Symposium. Cranfield, pp. 76–94.

Garud, Y.S., 1981. Multiaxial fatigue: A survey of the state of the art. Journal of Testing and Evaluation 9, 165–178.

Hou, Y.-C., Ling, J., Pan, J., 1998. Effects of bushing models on fatigue life assessment of an automotive structural component based on multiaxial fatigue theories. Computer Modeling and Simulation in Engineering, in press.

Il'yushin, A.A., 1946. The theory of small elastic–plastic deformations. Prikadnaia Matematika i Mekhanika 10, 347–356.

Kandil, F.A., Brown, M.W., Miller, K.J., 1982. Biaxial low-cycle fatigue of 316 stainless steel at elevated temperatures. Mechanical Behaviour and Nuclear Applications of Stainless Steel at Elevated Temperatures. The Metals Society, London, pp. 203–210.

Lohr, R.D., Ellison, E.G., 1980. A simple theory for low cycle multiaxial fatigue. Fatigue of Engineering Materials and Structures 3, 1–17.

O'Dowd, N.P., Shih, C.F., 1991. Family of crack-tip fields characterized by a triaxiality parameter—I. Structure of fields. Journal of the Mechanics and Physics of Solids 39, 989–1015.

O'Dowd, N.P., Shih, C.F., 1992. Family of crack-tip fields characterized by a triaxiality parameter-II. Fracture applications. Journal of the Mechanics and Physics of Solids 40, 939–963.

Rice, J.R., 1968. A path independent integral and the approximate analysis of strain concentration by notches and cracks. Journal of Applied Mechanics 35, 379–386.

Shih, C.F., 1973. Elastic–plastic analysis of combined mode crack problems. Ph.D. thesis, Harvard University, Cambridge, MA.

Socie, D.F., 1993. Critical plane approaches for multiaxial fatigue damage assessment. Advances in Multiaxial Fatigue, ASTM STP 1191. American Society of Testing and Materials, Philadelphia, pp. 7–36.

Socie, D.F., Waill, L.A., Dittmer, D.F., 1985. Biaxial fatigue of inconel 718 including mean stress effects. Multiaxial Fatigue, ASTM STP 853. American Society of Testing and Materials, Philadelphia, pp. 463–481.

Wang, Y., Pan, J., 1996a. Characterization of low-cycle multiaxial fatigue by a plastic fracture mechanics model. Fatigue and Fracture, 1996, Vol. 1, PVP-Vol. 323. ASME, New York, pp. 317–322.

Wang, Y., Pan, J., 1996b. Mixed-mode crack-tip fields under general yielding conditions and implications to low-cycle multiaxial fatigue theory. In: Chang, J.C.I., et al. (Eds.), Proceedings of the ASME Aerospace Division, AD-Vol. 52. The 1996 International Mechanical Engineering Congress and Exposition, Atlanta, pp. 269–279.

Wang, Y., Pan, J. 1998a. A plastic fracture mechanics analysis of small Case B fatigue cracks under multiaxial loading conditions, presented at ASME TURBO EXPO '97—Land, Sea, and Air—42nd Gas Turbine and Aeroengine Congress, Users' Symposium and Exposition, Paper Number 97-GT-237. Journal of Engineering for Gas Turbine and Power, to appear.

Wang, Y., Pan, J., 1998b. A plastic fracture mechanics model for characterization of multiaxial low-cycle fatigue. International Journal of Fatigue 20, 775–784.